

Reexamination of spin decoherence in semiconductor quantum dots from equation-of-motion approach

Y. Y. Wang,^{1,2} J. H. Jiang,² and M. W. Wu^{1,2,*}

¹*Hefei National Laboratory for Physical Sciences at Microscale,*

University of Science and Technology of China, Hefei, Anhui, 230026, China

²*Department of Physics, University of Science and Technology of China, Hefei, Anhui, 230026, China[†]*

(Dated: March 20, 2014)

The longitudinal and transversal spin relaxation times, T_1 and T_2 , in semiconductor quantum dots are investigated for different well widths, magnetic fields and quantum dot diameters. Various mechanisms, such as the hyperfine interaction with the surrounding nuclei, the Dresselhaus spin-orbit coupling together with the electron-bulk-phonon interaction, the g -tensor fluctuations, the direct spin-phonon coupling due to the phonon-induced strain, and the coaction of the electron-bulk/surface-phonon interaction together with the hyperfine interaction are included. The relative contributions from these spin decoherence mechanisms are compared in detail. In our calculation, the spin-orbit coupling is included in each mechanism and is shown to have marked effect in most cases. The equation-of-motion approach is applied in studying both the spin relaxation and the spin dephasing, both in Markovian and non-Markovian limits. We also show that the Fermi golden rule approach is only valid in calculating the spin relaxation with small spin-orbit coupling and around zero temperature. We also compare the relative magnitude of T_1 and T_2 and show that around zero temperature, $T_2 = 2T_1$. However, when the temperature is increased, T_1/T_2 is increased strongly.

PACS numbers: 72.25.Rb, 73.21.La, 71.70.Ej

I. INTRODUCTION

One of the most important issues in the growing field of spintronics is quantum information processing in quantum dots (QDs) using electron spin.^{1,2,3,4,5} A main obstacle is that the electron spin is unavoidably coupled to the environment (such as, the lattice) which leads to considerable spin decoherence (including longitudinal and transversal spin relaxation). Various mechanisms, such as, the hyperfine interaction with the surrounding nuclei,^{6,7} the Dresselhaus/Rashba spin-orbit coupling (SOC)^{8,9} together with the electron-phonon interaction, g -tensor fluctuations,¹⁰ the direct spin-phonon coupling due to the phonon-induced strain,¹¹ and the coaction of the hyperfine interaction and the electron-phonon interaction can lead to the spin decoherence. There are quite a lot of theoretical works on spin decoherence in single QD. Specifically, Khaetskii and Nazarov analyzed the spin-flip transition rate using a perturbative approach due to the SOC together with the electron-phonon interaction, g -tensor fluctuations, the direct spin-phonon coupling due to the phonon-induced strain qualitatively.^{12,13,14} After that, the longitudinal spin relaxation time T_1 due to the Dresselhaus and/or the Rashba SOC together with the electron-phonon interaction were studied quantitatively in Refs. 15,16,17,18,19,20,21. Among these works, Cheng *et al.*¹⁷ developed an exact diagonalization method and showed that due to the strong SOC, the previous perturbation method^{12,14,15} is inadequate in describing T_1 . Furthermore, they also showed that, the perturbation method previously used missed an important second-order energy correction and would yield qualitatively wrong results if the energy correction is correctly included and only the lowest few states are kept as those

in Refs. 12,14,15. These results were later confirmed by Destefani and Ulloa.²⁰ The contribution of the coaction of the hyperfine interaction and the electron-phonon interaction to longitudinal spin relaxation was calculated in Refs. 22 and 23. In contrast to the longitudinal spin relaxation time, there are relatively fewer works on the transversal spin relaxation time, T_2 , also referred to as the spin dephasing time (while the longitudinal spin relaxation time is referred to as the spin relaxation time for short). The spin dephasing time due to the Dresselhaus and/or the Rashba SOC together with the electron-phonon interaction was studied by Semenov and Kim²⁴ and by Golovach *et al.*¹⁹ The contributions of the hyperfine interaction and of the g -factor fluctuation were studied in Refs. 25,26,27,28,29,30,31,32,33,34 and in Ref. 35 respectively. However, a quantitative calculation of the strain-induced electron spin decoherence in a single QD is still lacking. This is one of the issues we are going to present in this paper. In brief, the spin relaxation/dephasing due to various mechanisms has been studied previously in many theoretical works. However, almost all of these works only focus individually on one mechanism. Although Khaetskii and Nazarov discussed the effects of different mechanisms on the spin relaxation time, their results are only qualitative and there is no comparison of the relative importance of the different mechanisms.^{12,13,14} To fully understand the microscopic mechanisms of spin relaxation and dephasing, and to achieve control over the spin coherence in QDs,^{36,37,38} one needs to gain insight into the relative importance of each mechanism to T_1 and T_2 under various conditions. This is one of the main purposes of this paper.

Another issue we are going to address relates to different approaches used in the study of the spin re-

laxation time. Previously, there have been two approaches in studying the spin relaxation time: the Fermi Golden rule, and the equation-of-motion method. Most of the previous works were performed using the first approach,^{12,13,14,15,16,17,18,20,22,23,39,40,41,42,43,44} while several authors used the latter one in dealing with two level systems.^{19,45,46} Due to SOC, each eigenstate of the electron Hamiltonian is a mixture of spin-up and -down states. The spin relaxation time between two states calculated via the Fermi Golden rule is in fact the spin relaxation time between two spin mixed states, instead of the one between pure spin-up and spin-down states. For weak SOC, a majority spin polarization can be defined, and one can therefore approximate the spin relaxation time between the spin-up and -down states to be the one between two mixed states with majority spin-up and -down. In this case, both approaches should yield similar results. However, when the SOC is large, defining the majority spin polarization becomes impossible, and the evaluation of the spin relaxation time using the Fermi Golden rule becomes inapplicable. For a stricter definition and calculation of spin relaxation and also dephasing, we solve the equation of motion of many-state systems directly. With a proper initial distribution, one can obtain the time evolution of the expectation value of spin. The spin relaxation (dephasing) is then well defined by the decay of $S_z(t)$ ($|S_z(t)|$). In this paper, we calculate the spin relaxation/dephasing time by the equation-of-motion approach. We compare the results obtained from the two approaches and show under what conditions the two methods yield the same results as well as under what conditions the Fermi-Golden-rule approach is inapplicable.

It is further noticed that Golovach *et. al.* have shown that the spin dephasing time T_2 is two times the spin relaxation time T_1 .¹⁹ However, as temperature increases, this relation does not hold. Semenov and Kim on the other hand reported that the spin dephasing time is much smaller than the spin relaxation time.²⁴ In this paper, we calculate the temperature dependence of the ratio of the spin relaxation time and the spin dephasing time and analyze the underlying physics.

This paper is organized as follows: In Sec. II, we present our model and formalism of the equation-of-motion approach. We also briefly introduce all the spin decoherence mechanisms considered in our calculations. In Sec. III we present our numerical results to indicate the contribution of each spin decoherence mechanism to spin relaxation/dephasing time under various conditions in single QDs based on the equation-of-motion approach. Then we investigate the difference between the Fermi Golden rule and the equation-of-motion approaches in Sec. IV. The temperature dependence of T_1/T_2 is investigated in Sec. V. We conclude in Sec. VI.

II. MODEL AND FORMALISM

A. Model and Hamiltonian

We consider a single QD system, where the QD is confined by a parabolic potential $V_c(x, y) = \frac{1}{2}m^*(x^2 + y^2)$ in the quantum well plane. The width of the quantum well is a . A magnetic field B is applied along the growth direction. The total Hamiltonian of the system of electron together with the lattice is:

$$H_T = H_e + H_L + H_{eL}, \quad (1)$$

where H_e , H_L , H_{eL} are the Hamiltonians of the electron, the lattice and their interaction, respectively. The electron Hamiltonian is given by

$$H_e = \frac{\mathbf{P}^2}{2m^*} + V_c(\mathbf{r}) + H_Z + H_{SO} \quad (2)$$

where $\mathbf{P} = -i\hbar\nabla + \frac{e}{c}\mathbf{A}$ with $\mathbf{A} = (\mathbf{B}/2)(-\mathbf{y}, \mathbf{x})$, $H_Z = \frac{1}{2}g\mu_B B\sigma_z$ is the Zeeman energy with μ_B the Bohr magneton, and H_{SO} is the Hamiltonian of SOC. In GaAs, when the quantum well width is small or the gate-voltage along the growth direction is small, the Rashba SOC is unimportant.⁴⁷ Therefore, only the Dresselhaus term⁸ contributes to H_{SO} . When the quantum well width is smaller than the QD radius, the dominant term in the Dresselhaus SOC reads

$$H_{so} = \frac{\gamma_0}{\hbar^3} \sum_{\lambda} \langle P_z^2 \rangle_{\lambda} (-P_x \sigma_x + P_y \sigma_y), \quad (3)$$

with γ_0 denoting the Dresselhaus coefficient, λ being the quantum number of z direction and $\langle P_z^2 \rangle_{\lambda} \equiv -\hbar^2 \int \psi_{z\lambda}^*(z) \partial^2 / \partial z^2 \psi_{z\lambda}(z) dz$. The Hamiltonian of the lattice consists of two parts $H_L = H_{ph} + H_{nuclei}$, where $H_{ph} = \sum_{\mathbf{q}\eta} \hbar\omega_{\mathbf{q}\eta} a_{\mathbf{q}\eta}^\dagger a_{\mathbf{q}\eta}$ (a^\dagger/a is the phonon creation/annihilation operator) describes the vibration of the lattice and $H_{nuclei} = \sum_j \gamma_I B I_{jz}$ (γ_I is the gyromagnetic ratios of the nuclei and I_{jz} is the z -component of spin of the j -th nucleus) describes the precession of the nuclei spins of the lattice in the external magnetic field. The interaction between the electron and the lattice also has two parts $H_{eL} = H_{eI} + H_{e-ph}$, where H_{eI} is the hyperfine interaction between the electron and nuclei and H_{e-ph} represents the electron-phonon interaction which is further composed of the electron-bulk-phonon (BP) interaction H_{ep} , strain-induced electron spin-phonon coupling H_{strain} and electron spin-phonon interaction due to the phonon-induced g -factor fluctuation H_g .

B. Equation-of-motion approach

The equations of motion can describe both the coherent and the dissipative dynamics of the electron system. When the quasi-particles of the bath relax much faster than the single electron system and the scattering between the electron and the quasi-particle of the bath is

weak, the Markovian approximation can be made; otherwise the kinetics is the non-Markovian. For electron-phonon coupling, due to the fast relaxation of the phonon bath and the weak electron-phonon scattering, the kinetics of the electron is Markovian. Nevertheless, as the nuclei spin bath relaxes much slower than the electron spin, the kinetics due to the coupling with nuclei is of non-Markovian type.²⁸ It is further noted that there is also a contribution from the coaction of the electron-phonon and electron-nuclei couplings, which is a fourth order coupling to the bath. For this contribution, the decoherence of spin is mainly controlled by the electron-phonon scattering while the nuclei acts as a static magnetic field. Thus, this fourth order coupling is also Markovian. Finally, since the electron orbit relaxation is much faster than the electron spin relaxation,⁴⁸ we always assume a thermo-equilibrium initial distribution of the orbital degrees of freedom.

1. Markovian kinetics

The equation of motion for the electron system coupled to the phonon bath can be obtained with the help of the projection operator technique,⁴⁹

$$\begin{aligned} \frac{d\rho^e(t)}{dt} = & -i[H_e + \text{Tr}_{ph}(H_{e-ph}\rho_{ph}^0), \rho^e(t)] \\ & - \int_0^t d\tau \text{Tr}_{ph}[H_{e-ph}, [H_{e-ph}^I(-\tau), U_0(\tau)\rho^e(t-\tau) \\ & \otimes \rho_{ph}^0 U_0^\dagger(\tau)]] , \end{aligned} \quad (4)$$

where ρ^e is the density operator of the electron system, Tr_{ph} means trace over the phonon degree of freedom, $H_{e-ph}^I(-\tau) = U_0(\tau)H_{e-ph}U_0^\dagger(\tau)$ with $U_0(\tau) = e^{-i(H_{ph}+H_e)\tau}$. ρ_{ph}^0 is the equilibrium distribution of the phonon bath. Hence $\text{Tr}_{ph}(H_{e-ph}\rho_{ph}^0) = 0$. Within the base of the eigenstates of the electron Hamiltonian, $\{|\ell\rangle\}$, Eq. (4) reads,

$$\begin{aligned} \frac{d}{dt}\rho_{\ell_1\ell_2}^e = & -i(\varepsilon_{\ell_1} - \varepsilon_{\ell_2})\rho_{\ell_1\ell_2}^e \\ & - \left\{ \frac{1}{\hbar^2} \int_0^t d\tau \sum_{\ell_3\ell_4} \text{Tr}_p(H_{\ell_1\ell_3}^{e-ph} H_{\ell_3\ell_4}^{Ie-ph} \rho_{\ell_4\ell_2}^e \otimes \rho_{eq}^p \right. \\ & \left. - H_{\ell_1\ell_3}^{Ie-ph} \rho_{\ell_3\ell_4}^e \otimes \rho_{eq}^p H_{\ell_4\ell_2}^{e-ph}) + H.c. \right\} . \end{aligned} \quad (5)$$

A general form of the electron-phonon interaction reads

$$H_{e-ph} = \sum_{\mathbf{q}\eta} \Phi_{\mathbf{q}\eta} (a_{\mathbf{q}\eta} + a_{-\mathbf{q}\eta}^\dagger) X_{\mathbf{q}\eta}(\mathbf{r}, \boldsymbol{\sigma}) . \quad (6)$$

Substituting this into Eq. (5), we obtain, after integration within the Markovian approximation,³⁸

$$\begin{aligned} \frac{d}{dt}\rho_{\ell_1\ell_2}^e = & i(\varepsilon_{\ell_1} - \varepsilon_{\ell_2})\rho_{\ell_1\ell_2}^e \\ & - \left\{ \frac{\pi}{\hbar^2} \sum_{\ell_3\ell_4} \sum_{\mathbf{q}\eta} |\Phi_{\mathbf{q}\eta}|^2 \{ X_{\ell_1\ell_3}^{\mathbf{q}\eta} X_{\ell_4\ell_3}^{\mathbf{q}\eta*} \rho_{\ell_4\ell_2}^e \right. \\ & \times C_{\mathbf{q}\eta}(\varepsilon_{\ell_4} - \varepsilon_{\ell_3}) - X_{\ell_4\ell_2}^{\mathbf{q}\eta} X_{\ell_3\ell_1}^{\mathbf{q}\eta*} \rho_{\ell_3\ell_4}^e \\ & \left. \times C_{\mathbf{q}\eta}(\varepsilon_{\ell_3} - \varepsilon_{\ell_1}) \right\} + H.c. \end{aligned} \quad (7)$$

in which $X_{\ell_1\ell_2}^{\mathbf{q}\eta} = \langle \ell_1 | X_{\mathbf{q}\eta}(\mathbf{r}, \boldsymbol{\sigma}) | \ell_2 \rangle$, and $C_{\mathbf{q}\eta}(\Delta\varepsilon) = \bar{n}(\omega_{\mathbf{q}\eta})\delta(\Delta\varepsilon + \omega_{\mathbf{q}\eta}) + [\bar{n}(\omega_{\mathbf{q}\eta}) + 1]\delta(\Delta\varepsilon - \omega_{\mathbf{q}\eta})$. Here $\bar{n}(\omega_{\mathbf{q}\eta})$ represents the Bose distribution function. Equation (7) can be written in a more compact form

$$\frac{d}{dt}\rho_{\ell_1\ell_2}^e = - \sum_{\ell_3\ell_4} \Lambda_{\ell_1\ell_2\ell_3\ell_4} \rho_{\ell_3\ell_4}^e , \quad (8)$$

which is a linear differential equation. This equation can be solved by diagonalizing Λ . Given an initial distribution $\rho_{\ell_1\ell_2}^e(0)$, the density matrix $\rho_{\ell_1\ell_2}^e(t)$ and any physical quantity $O(t) = \text{Tr}(\hat{O}\rho^e(t))$ at time t can be obtained:³⁸

$$\begin{aligned} O(t) = & \text{Tr}(\hat{O}\rho^e) \\ = & \sum_{\ell_1 \dots \ell_6} \langle \ell_2 | \hat{O} | \ell_1 \rangle \mathbf{P}_{(\ell_1\ell_2)(\ell_3\ell_4)} \\ & \times e^{-\mathbf{\Gamma}_{(\ell_3\ell_4)} t} \mathbf{P}_{(\ell_3\ell_4)(\ell_5\ell_6)}^{-1} \rho_{\ell_5\ell_6}^e(0) \end{aligned} \quad (9)$$

with $\mathbf{\Gamma} = \mathbf{P}^{-1}\mathbf{\Lambda}\mathbf{P}$ being the diagonal matrix and \mathbf{P} representing the transformation matrix. To study spin dynamics, we calculate $S_z(t)$ ($|S_+(t)|$) and define the spin relaxation (dephasing) time as the time where S_z ($|S_+|$) decays to $1/e$ of its initial value.

2. Non-Markovian kinetics

For the hyperfine interaction induced spin dephasing, the Markovian approximation cannot be made because the relaxation of the nuclei spin bath is larger than the electron spin dephasing time.²⁸ The hyperfine interaction Hamiltonian can be written as $H_{eI} = \mathbf{h} \cdot \mathbf{S}$ with $\mathbf{h} = \sum_j A v_0 \mathbf{I}_j \delta(\mathbf{r} - \mathbf{R}_j)$. Any state of the nuclear spin system $|n\rangle$ can be expanded as

$$|n\rangle = \sum_{m_1 \dots m_N} \alpha_{m_1 \dots m_N}^n \bigotimes_{j=1}^N |I, m_j\rangle , \quad (10)$$

where $|I, m_j\rangle$ is the eigenstate of the z -component of the j -th nucleus I_{jz} with the eigenvalue m_j . N denotes the number of the nuclei spin. For a certain orbital state $|\psi_k\rangle$ of the electron, the hyperfine field is $\mathbf{h}_k = \langle \psi_k | \mathbf{h} | \psi_k \rangle = \sum_j A v_0 \mathbf{I}_j |\psi_k(\mathbf{R}_j)|^2$. In the following, the matrix element $\langle n | \mathbf{h}_k | n' \rangle$ is denoted as $[\mathbf{h}]_{knn'}$ for short. Bearing these in mind, we now discuss the

non-Markovian equation of motion due to the hyperfine interaction. The equation of motion is similar to Eq. (4). One only needs to replace the electron-phonon interaction with the hyperfine interaction and the phonon bath with the nuclei spin bath. Considering an unpolarized nuclei spin bath with the equilibrium distribution $\rho_I^0 = \sum_n w_n |n\rangle\langle n|$, where the probability $w_n = 1/N_w$ with $N_w = \sum_n 1$ being the number of all possible states of the nuclear spin system, *i.e.* each state has equal probability and assuming a thermo-equilibrium distribution of the orbital degrees of freedom, we obtain the equation for $\langle S_+ \rangle_t$ ($\equiv \langle S_x \rangle_t + i\langle S_y \rangle_t$)

$$\frac{d}{dt}\langle S_+ \rangle_t = i \sum_{kn} f_k w_n \omega_{kn} \langle S_+ \rangle_t - i \int_0^t dt' \Sigma_{++}(t-t') \langle S_+ \rangle_{t'}, \quad (11)$$

where $\omega_{kn} = g\mu_B B + [h_z]_{knn}$ and $\langle \dots \rangle = \text{Tr}(\rho^e \dots)$. The $[h_z]_{knn}$ term in the coherent part of the equation of motion comes from the $\text{Tr}_{nuclei}(H_{eI}\rho_I^0)$ in Eq. (4), which is an Overhauser shift. For an unpolarized nuclei spin bath, the Overhauser shift $\sum_n w_n [h_z]_{knn}$ is zero. Similar equation has been obtained by Coish and Loss,²⁸ and later by Deng and Hu³⁰ for very low temperature such that only the lowest two Zeeman sublevels need to be considered. In their work Coish and Loss also presented an efficient way to evaluate $\Sigma_{++}(t)$ in terms of their Laplace transformations, $f(s) = \int_0^\infty dt e^{-st} f(t)$. By using their technique, we obtain

$$\Sigma_{++}(s) = -\frac{i}{4} \sum_{knn'} f_k w_n ([h_+]_{knn'} [h_-]_{kn'n} + [h_-]_{knn'} [h_+]_{kn'n}) / (s - i\delta\omega_{knn'}) , \quad (12)$$

with $\delta\omega_{knn'} = \frac{1}{2}(\omega_{kn} - \omega_{kn'})$. The electron spin dephasing time is then defined as the time at which the envelop of $|S_+|$ decays to $1/e$ of its initial value.

C. Spin decoherence mechanisms

In this subsection we briefly summarize all the spin decoherence mechanisms. It is noted that the SOC modifies all the mechanisms. This is because the SOC modifies the Zeeman splitting¹⁷ and the spin-resolved eigenstates of the electron Hamiltonian, it hence greatly changes the effect of the electron-BP scattering.¹⁷ These two modifications, especially the modification of the Zeeman splitting, also change the effect of other mechanisms, such as, the spin-phonon coupling due to the phonon-induced strain, the g -factor fluctuation, the coaction of the electron-phonon interaction and the hyperfine interaction. In the literature, except for the electron-BP scattering, the effects from the SOC are neglected except for the work by Woods *et. al.*¹⁵ in which the spin relaxation time between the two Zeeman sub-levels of the lowest electronic state

due to the phonon-induced strain is investigated. However, the perturbation method they used does not include the important second-order energy correction. In our investigation, the effects of the SOC are included in all the mechanisms and we will show that they sometimes lead to marked effects.

1. SOC together with electron-phonon scattering

As the SOC mixes different spins, the electron-BP scattering can induce spin relaxation and dephasing. The electron-BP coupling is given by

$$H_{ep} = \sum_{\mathbf{q}\eta} M_{\mathbf{q}\eta} (a_{\mathbf{q}\eta} + a_{-\mathbf{q}\eta}^\dagger) e^{i\mathbf{q}\cdot\mathbf{r}} , \quad (13)$$

where $M_{\mathbf{q}\eta}$ is the matrix element of the electron-phonon interaction. In the general form of the electron phonon interaction H_{e-ph} , $\Phi_{\mathbf{q}\eta} = M_{\mathbf{q}\eta}$ and $X_{\mathbf{q}\eta}(\mathbf{r}, \boldsymbol{\sigma}) = e^{i\mathbf{q}\cdot\mathbf{r}}$. $|M_{\mathbf{q}sl}|^2 = \hbar \Xi^2 q / 2\rho v_{sl} V$ for the electron-BP coupling due to the deformation potential. For the piezoelectric coupling, $|M_{\mathbf{q}pl}|^2 = (32\hbar\pi^2 e^2 e_{14}^2 / \kappa^2 \rho v_{sl} V) [(3q_x q_y q_z)^2 / q^7]$ for the longitudinal phonon mode and $\sum_{j=1,2} |M_{\mathbf{q}pt_j}|^2 = [32\hbar\pi^2 e^2 e_{14}^2 / (\kappa^2 \rho v_{st} q^5 V)] [q_x^2 q_y^2 + q_y^2 q_z^2 + q_z^2 q_x^2 - (3q_x q_y q_z)^2 / q^2]$ for the two transverse modes. Here Ξ stands for the acoustic deformation potential; ρ is the GaAs volume density; V is the volume of the lattice; e_{14} is the piezoelectric constant and κ denotes the static dielectric constant. The acoustic phonon spectra $\omega_{\mathbf{q}l} = v_{sl} q$ for the longitudinal mode and $\omega_{\mathbf{q}t} = v_{st} q$ for the transverse mode with v_{sl} and v_{st} representing the corresponding sound velocities. This mechanism contributes to both spin relaxation and dephasing. It has been shown that at low temperature the spin dephasing time is two times the spin relaxation time.¹⁹ However, as temperature increases this relation does not hold. We will study the ratio of the two and reveal the underlying physics in Sec. V.

Beside the electron-BP scattering, electron also couples to vibrations of the confining potential, *i.e.*, the surface-phonons,²³

$$\delta V(\mathbf{r}) = - \sum_{\mathbf{q}\eta} \sqrt{\frac{\hbar}{2\rho\omega_{\mathbf{q}\eta} V}} (a_{\mathbf{q}\eta} + a_{-\mathbf{q}\eta}^\dagger) \boldsymbol{\epsilon}_{\mathbf{q}\eta} \cdot \nabla_{\mathbf{r}} V_c(\mathbf{r}) , \quad (14)$$

in which $\boldsymbol{\epsilon}_{\mathbf{q}\eta}$ is the polarization vector of a phonon mode with wavevector \mathbf{q} in branch η . However, this contribution is much smaller than the electron-BP coupling. Compared to the coupling due to the deformation potential for example, the ratio of the two coupling strengths is $\approx \hbar\omega_0 / \Xi q l_0$, where l_0 is the characteristic length of the quantum dot and $\hbar\omega_0$ is the orbital level splitting. The phonon wavevector q is determined by the energy difference between the final and initial states of the transition. Typically phonon transitions between Zeeman sublevels and different orbital levels, $q l_0$ ranges from 0.1 to 10. Bearing in mind that $\hbar\omega_0$ is about 1 meV while $\Xi = 7$ eV

in GaAs, $\hbar\omega_0/\Xi ql_0$ is about 10^{-3} . The piezoelectric coupling is of the same order as the deformation potential. Therefore spin decoherence due to the electron-surface-phonon coupling is negligible.

2. Direct spin-phonon coupling due to phonon-induced strain

The direct spin-phonon coupling due to the phonon-induced strain is given by⁵⁰

$$H_{strain} = \frac{1}{2} \mathbf{h}^s(\mathbf{p}) \cdot \boldsymbol{\sigma}, \quad (15)$$

where $h_x^s = -Dp_x(\epsilon_{yy} - \epsilon_{zz})$, $h_y^s = -Dp_y(\epsilon_{zz} - \epsilon_{xx})$ and $h_z^s = -Dp_z(\epsilon_{xx} - \epsilon_{yy})$ with $\mathbf{p} = (p_x, p_y, p_z) = -i\hbar\nabla$ and D being the material strain constant. ϵ_{ij} ($i, j = x, y, z$) can be expressed by the phonon creation and annihilation operators:

$$\epsilon_{ij} = \sum_{\mathbf{q}\eta=l,t_1,t_2} \frac{i}{2} \sqrt{\frac{\hbar}{2\rho\omega_{\mathbf{q}\eta}V}} (a_{\mathbf{q},\eta} + a_{-\mathbf{q},\eta}^\dagger) (\xi_{i\eta}q_j + \xi_{j\eta}q_i) e^{i\mathbf{q}\cdot\mathbf{r}}, \quad (16)$$

in which $\xi_{il} = q_i/q$ for the longitudinal phonon mode and $(\xi_{xt_1}, \xi_{yt_1}, \xi_{zt_1}) = (q_xq_z, q_yq_z, -q_\parallel^2/qq_\parallel)$, $(\xi_{xt_2}, \xi_{yt_2}, \xi_{zt_2}) = (q_y, -q_x, 0)/q_\parallel$ for the two transverse phonon modes with $q_\parallel = \sqrt{q_x^2 + q_y^2}$. Therefore, in the general form of electron-phonon interaction H_{e-ph} , $\Phi_{\mathbf{q}\eta} = -iD\sqrt{\hbar/(32\rho\omega_{\mathbf{q}\eta}V)}$ and $X_{\mathbf{q}\eta}(\mathbf{r}, \boldsymbol{\sigma}) = \sum_{ijk} \epsilon_{ijk} (\xi_{j\eta}q_k - \xi_{k\eta}q_j) p_i e^{i\mathbf{q}\cdot\mathbf{r}} \sigma_i$ with ϵ_{ijk} denoting the Levi-Civita tensor.

3. g -factor fluctuation

The spin-lattice interaction via phonon modulation of the g -factor is given by³⁹

$$H_g = \frac{\hbar}{2} \sum_{ijkl=x,y,z} A_{ijkl} \mu_B B_i \sigma_j \epsilon_{kl}, \quad (17)$$

where ϵ_{kl} is given in Eq. (16) and A_{ijkl} is a tensor determined by the material. Therefore in H_{e-ph} , $\Phi_{\mathbf{q}\eta} = i\sqrt{\hbar/(32\rho\omega_{\mathbf{q}\eta}V)}$ and $X_{\mathbf{q}\eta}(\mathbf{r}, \boldsymbol{\sigma}) = \sum_{i,j,k,l} A_{i,j,k,l} \mu_B B_i (\xi_{k\eta}q_l - \xi_{l\eta}q_k) \sigma_j e^{i\mathbf{q}\cdot\mathbf{r}}$. Due to the axial symmetry with respect to the z -axis, and keeping in mind that the external magnetic field is along the z direction, the only finite element of H_g is $H_g = [(A_{33} - A_{31})\epsilon_{zz} + A_{31} \sum_i \epsilon_{ii}] \hbar \mu_B B \sigma_z / 2$ with $A_{33} = A_{zzzz}$, $A_{31} = A_{zzxx}$ and $A_{66} = A_{xyxy}$. $A_{33} + 2A_{31} = 0$.³⁵

4. Hyperfine interaction

The hyperfine interaction between the electron and nuclei spins is⁵¹

$$H_{eI}(\mathbf{r}) = \sum_j A v_0 \mathbf{S} \cdot \mathbf{I}_j \delta(\mathbf{r} - \mathbf{R}_j), \quad (18)$$

where $\mathbf{s} = \hbar\boldsymbol{\sigma}/2$ and \mathbf{I}_j are the electron and nucleus spins respectively, $v_0 = a_0^3$ is the volume of the unit cell with a_0 representing the crystal lattice parameter, and \mathbf{r} (\mathbf{R}_j) denotes the position of the electron (the j -th nucleus). $A = 4\mu_0\mu_B\mu_I/(3Iv_0)$ is the hyperfine coupling constant with μ_0 , μ_B and μ_I representing the permeability of vacuum, the Bohr magneton and the nuclear magneton separately.

As the Zeeman splitting of the electron is much larger (three orders of magnitude larger) than that of the nucleus spin, to conserve the energy for the spin relaxation processes, there must be phonon-assisted transitions when considering the spin-flip processes. Taking into account directly the BP induced motion of nuclei spin of the lattice leads to a new spin relaxation mechanism.²³

$$V_{eI-ph}^{(1)}(\mathbf{r}) = - \sum_j A v_0 \mathbf{S} \cdot \mathbf{I}_j (\mathbf{u}(\mathbf{R}_j^0) \cdot \nabla_{\mathbf{r}}) \delta(\mathbf{r} - \mathbf{R}_j), \quad (19)$$

where $\mathbf{u}(\mathbf{R}_j^0) = \sum_{\mathbf{q}\eta} \sqrt{\hbar/(2\rho\omega_{\mathbf{q}\eta}v_0)} (a_{\mathbf{q}\eta} + a_{\mathbf{q}\eta}^\dagger) \epsilon_{\mathbf{q}\eta} e^{i\mathbf{q}\cdot\mathbf{R}_j^0}$ is the lattice displacement vector. Therefore using the notation of Eq. (6), $\Phi = \sqrt{\hbar/(2\rho V\omega_{\mathbf{q}\eta})}$ and $X_{\mathbf{q}\eta} = \sum_j A v_0 \mathbf{S} \cdot \mathbf{I}_j \nabla_{\mathbf{r}} \delta(\mathbf{r} - \mathbf{R}_j)$. The second-order process of the surface phonon and the BP together with the hyperfine interaction also leads to spin relaxation:

$$V_{eI-ph}^{(2)}(\mathbf{r}) = \sum_{m \neq \ell_1 \ell_2} |\ell_2\rangle \left[\frac{\langle \ell_2 | \delta V_c(\mathbf{r}) | m \rangle \langle m | H_{eI}(\mathbf{r}) | \ell_1 \rangle}{\varepsilon_{\ell_1} - \varepsilon_m} + \frac{\langle \ell_2 | H_{eI}(\mathbf{r}) | m \rangle \langle m | \delta V_c(\mathbf{r}) | \ell_1 \rangle}{\varepsilon_{\ell_2} - \varepsilon_m} \right] \langle \ell_1 |, \quad (20)$$

and

$$V_{eI-ph}^{(3)} = \sum_{m \neq \ell_1 \ell_2} |\ell_2\rangle \left[\frac{\langle \ell_2 | H_{ep} | m \rangle \langle m | H_{eI}(\mathbf{r}) | \ell_1 \rangle}{\varepsilon_{\ell_1} - \varepsilon_m} + \frac{\langle \ell_2 | H_{eI}(\mathbf{r}) | m \rangle \langle m | H_{ep} | \ell_1 \rangle}{\varepsilon_{\ell_2} - \varepsilon_m} \right] \langle \ell_1 |, \quad (21)$$

in which $|\ell_1\rangle$ and $|\ell_2\rangle$ are the eigen states of H_e . Therefore using the notations in H_{e-ph} , $\Phi_{\mathbf{q}\eta} = \frac{i}{\hbar} \sqrt{\hbar/(2\rho\omega_{\mathbf{q}\eta}v_0)}$ and

$$\begin{aligned} X_{\mathbf{q}\eta} &= |\ell_2\rangle \epsilon_{\mathbf{q}\eta} \cdot \sum_{m \neq \ell_1 \ell_2} \left\{ \frac{1}{\varepsilon_{\ell_1} - \varepsilon_m} \langle \ell_2 | [H_e, \mathbf{P}] | m \rangle \sum_j A v_0 \right. \\ &\quad \times \langle m | \mathbf{S} \cdot \mathbf{I}_j \delta(\mathbf{r} - \mathbf{R}_j) | \ell_1 \rangle + \frac{1}{\varepsilon_{\ell_2} - \varepsilon_m} \langle m | [H_e, \mathbf{P}] | \ell_1 \rangle \\ &\quad \times \sum_j A v_0 \langle \ell_2 | \mathbf{S} \cdot \mathbf{I}_j \delta(\mathbf{r} - \mathbf{R}_j) | m \rangle \left. \right\} \langle \ell_1 | \end{aligned} \quad (22)$$

for $V_{eI-ph}^{(2)}$. Similarly $\Phi_{q\eta} = M_{q\eta}$ and

$$\begin{aligned} X_{q\eta} = & |\ell_2\rangle \sum_{m \neq \ell_1 \ell_2} \left\{ \frac{\langle \ell_2 | e^{i\mathbf{q} \cdot \mathbf{r}} | m \rangle}{\varepsilon_{\ell_1} - \varepsilon_m} \sum_j A v_0 \langle m | \mathbf{S} \cdot \mathbf{I}_j \right. \\ & \times \delta(\mathbf{r} - \mathbf{R}_j) | \ell_1 \rangle + \frac{1}{\varepsilon_{\ell_2} - \varepsilon_m} \langle m | e^{i\mathbf{q} \cdot \mathbf{r}} | \ell_1 \rangle \\ & \left. \times \sum_j A v_0 \langle \ell_2 | \mathbf{S} \cdot \mathbf{I}_j \delta(\mathbf{r} - \mathbf{R}_j) | m \rangle \right\} \langle \ell_1 | \end{aligned} \quad (23)$$

for $V_{eI-ph}^{(3)}$. Again as the contribution from the surface phonon is much smaller than that of the BP, $V_{eI-ph}^{(2)}$ can be neglected. It is noted that, the direct spin-phonon coupling due to the phonon-induced strain together with the hyperfine interaction gives a fourth-order scattering and hence induces a spin relaxation/dephasing. The interaction is

$$\begin{aligned} V_{eI-ph}^{(4)} = & \sum_m |\ell_2\rangle \left[\frac{\langle \ell_2 | H_{strain}^z | m \rangle \langle m | V_{eI}(\mathbf{r}) | \ell_1 \rangle}{\varepsilon_{\ell_1} - \varepsilon_m} \right. \\ & \left. + \frac{\langle \ell_2 | \delta V_{eI}(\mathbf{r}) | m \rangle \langle m | H_{strain}^z | \ell_1 \rangle}{\varepsilon_{\ell_2} - \varepsilon_m} \right] \langle \ell_1 |, \end{aligned} \quad (24)$$

with $H_{strain}^z = h_s^z \sigma_z / 2$ only changing the electron energy but conserving the spin polarization. It can be written as

$$\frac{1}{2} h_s^z = -\frac{i}{2} D \sum_{q\eta} \sqrt{\frac{\hbar}{2\rho\omega_{q,\eta} V}} (\xi_{y\eta} q_y - \xi_{z\eta} q_z) q_z e^{i\mathbf{q} \cdot \mathbf{r}}. \quad (25)$$

Comparing this to the electron-BP interaction Eq. (13), the ratio is $\approx \hbar D q / \Xi$, which is about 10^{-3} . Therefore, the second-order term of the direct spin-phonon coupling due to the phonon-induced strain together with the hyperfine interaction is very small and can be neglected. Also the coaction of the g -factor fluctuation and the hyperfine interaction is very small compared to that of the electron-BP interaction jointly with the hyperfine interaction as $\mu_B B / \Xi$ is around 10^{-5} when $B = 1$ T. Therefore it can also be neglected. Therefore, in the following, we only retain the first and the third order terms $V_{eI-ph}^{(1)}$ and $V_{eI-ph}^{(3)}$ in calculating the spin relaxation time.

The spin dephasing time induced by the hyperfine can be calculated from the non-Markovian kinetic Eq. (11), resulting in

$$|\langle S_+ \rangle_t| \propto \sum_k f_k A^2 v_0^2 \int d\mathbf{r} |\psi_k(\mathbf{r})|^4 \cos\left(\frac{A v_0}{2} |\psi_k(\mathbf{r})|^2 t\right), \quad (26)$$

where f_k is the thermo-equilibrium distribution of the orbital degree of freedom. We then define the time when the envelop of $|\langle S_+ \rangle_t| / |\langle S_+ \rangle_0|$ equals $1/e$ as the spin dephasing time T_2 . As mentioned above the hyperfine interaction can not transfer an energy of the order of the Zeeman splitting, thus the hyperfine interaction alone can not lead to any spin relaxation.

III. SPIN DECOHERENCE DUE TO DIFFERENT MECHANISMS

Following the equation-of-motion approach developed in Sec. II, we perform a numerical calculation of the spin relaxation and dephasing times in GaAs QDs. The temperature is taken to be $T = 4$ K unless otherwise specified. When calculating T_1 , the initial distribution is taken to be in the spin majority down state of the eigen-state of the Hamiltonian H_e with a Maxwell-Boltzmann distribution $f_k = C \exp[-\epsilon_k / (k_B T)]$ for different orbital levels (C is the normalization constant). For the calculation of T_2 , we assign the same distribution between different orbital levels, but with a superposition of the two spin states within the same orbital level. The parameters used in the calculation are listed in Table I.^{6,52,53}

TABLE I: Parameters used in the calculation

ρ	$5.3 \times 10^3 \text{ kg/m}^3$	κ	12.9
v_{st}	$2.48 \times 10^3 \text{ m/s}$	g	-0.44
v_{sl}	$5.29 \times 10^3 \text{ m/s}$	Ξ	7.0 eV
e_{14}	$1.41 \times 10^9 \text{ V/m}$	m^*	$0.067 m_0$
A	90 μeV	A_{33}	19.6
τ_{ph}	$2.4 \times 10^{-8} \text{ s}$	I	$\frac{3}{2}$
D	$1.59 \times 10^4 \text{ m/s}$	a_0	5.6534 \AA
γ_0	27.5 $\text{\AA}^3 \cdot \text{eV}$		

A. Spin Relaxation Time T_1

We first study the spin relaxation time and show how it changes with the well width a , the magnetic field B and the effective diameter $d_0 = \sqrt{\hbar\pi/m^*\omega_0}$. We also compare the relative contributions from each relaxation mechanism.

1. Well width dependence

In Fig. 1 the spin relaxation times induced by different mechanisms are plotted as function of the width of the quantum well in which the QD is confined. In the calculation we take $B = 0.5$ T and $d_0 = 20$ nm. It is interesting to see that when the well width is small (smaller than 7 nm in the present case), the spin relaxation time is determined by the electron-BP scattering together with the SOC. However, for wider well widths, the direct spin-phonon coupling due to the strain and the nuclear hyperfine interaction combined with the electron-BP scattering becomes important. As we have mentioned earlier, this is because the electron-BP scattering itself cannot induce any spin flip and therefore cannot lead to spin relaxation. In the presence of SOC, however,

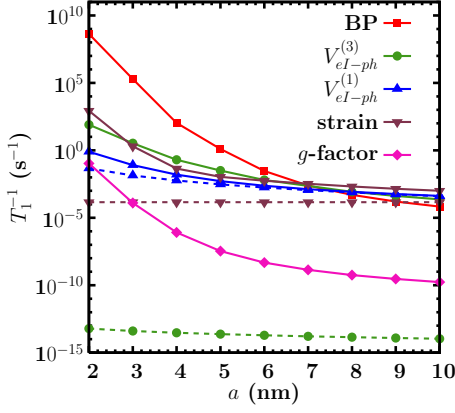


FIG. 1: (Color online) T_1^{-1} induced by different mechanisms with (solid curves) and without (dashed curves) the SOC vs. the well width at $B = 0.5$ T and $d_0 = 20$ nm. $T = 4$ K. Curve with \blacksquare — T_1^{-1} induced by the electron-BP scattering together with the SOC; Curves with \bullet — T_1^{-1} induced by the second-order process of the hyperfine interaction together with the BP ($V_{el}^{(3)}$); Curves with \blacktriangle — T_1^{-1} induced by the first-order process of the hyperfine interaction together with the BP ($V_{el}^{(1)}$); Curves with \blacktriangledown — T_1^{-1} induced by the direct spin-phonon coupling due to the strain; Curve with \blacklozenge — T_1^{-1} induced by the g -tensor fluctuation.

this mechanism can lead to spin relaxation. H_{SO} decreases with a as $H_{SO} \propto a^{-2}$. The other two scatterings, however, can lead to spin flip themselves even without the SOC. Therefore, the spin relaxation induced by the electron-BP scattering together with the SOC decreases faster with increasing well width compared to those induced by the other two mechanisms. It is also noted that the spin relaxation time due to the g -tensor fluctuation is two orders of magnitude smaller than that due to the leading spin decoherence mechanism and can therefore be neglected.

It is noted that in the calculation, the SOC is always included as it has large effect on the eigen-energy and eigen-wavefunction of the electron. We also show the spin relaxation times induced by the hyperfine interactions and the direct spin-phonon coupling due to the strain but without the SOC as in the literature.^{22,23,35} It can be seen clearly that the spin relaxation that includes the SOC is larger than that without the SOC. Especially, the spin relaxation induced by the second-order process of the hyperfine interaction together with the BP ($V_{el-ph}^{(3)}$) is at least 9 orders of magnitude larger when the SOC is included than that when the SOC is neglected. This is because when the SOC is neglected, $\langle m|H_{eI}(\mathbf{r})|\ell_1\rangle$ and $\langle \ell_2|H_{eI}(\mathbf{r})|m\rangle$ in Eq. (21) are very tiny as the matrix elements of $H_{eI}(\mathbf{r})$ between different orbital energy levels are very small. However, when the SOC is taken into account, the spin-up and -down levels with different orbital quantum numbers are mixed and therefore $|\ell\rangle$ and $|m\rangle$ include the components with the same orbital

quantum number. Consequently the matrix elements of $\langle m|H_{eI}(\mathbf{r})|\ell_1\rangle$ and $\langle \ell_2|H_{eI}(\mathbf{r})|m\rangle$ become large.

It is emphasized from the above discussion that the SOC has to be included in each spin relaxation mechanism. In the following calculations it is always included unless otherwise specified. In particular in reference to the electron-BP interaction, we always consider it together with the SOC.

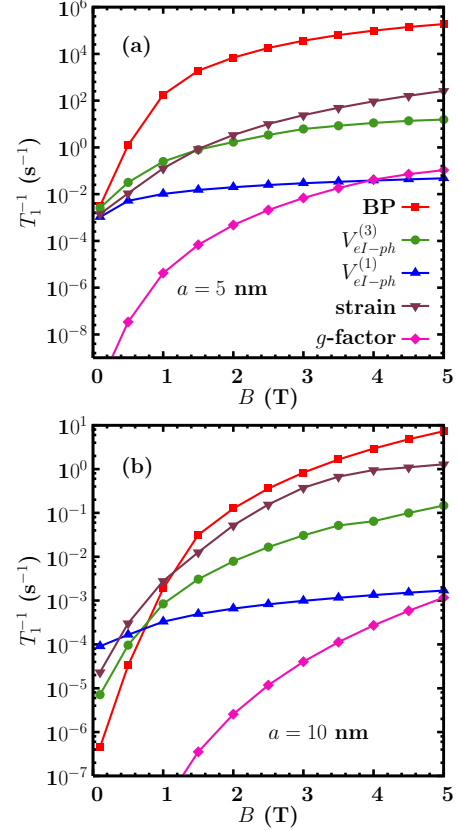


FIG. 2: (Color online) T_1^{-1} induced by different mechanisms vs. the magnetic field B at $d_0 = 20$ nm and (a) $a = 5$ nm and (b) 10 nm. $T = 4$ K. Curves with \blacksquare — T_1^{-1} induced by the electron-BP scattering; Curves with \bullet — T_1^{-1} induced by the second-order process of the hyperfine interaction together with the BP ($V_{el}^{(3)}$); Curves with \blacktriangle — T_1^{-1} induced by the first-order process of the hyperfine interaction together with the BP ($V_{el}^{(1)}$); Curves with \blacktriangledown — T_1^{-1} induced by the direct spin-phonon coupling due to the strain; Curves with \blacklozenge — T_1^{-1} induced by the g -tensor fluctuation.

2. Magnetic Field Dependence

We investigate the magnetic field dependence of T_1 at two different well widths as shown in Fig. 2. In the calculation, $d_0 = 20$ nm. It can be seen that for small well width (5 nm in Fig. 2a), the spin relaxation induced by the electron-BP scattering is dominant except at very

low magnetic fields (0.1 T in the figure) where contributions from the hyperfine interaction and the strain induced direct spin-phonon scattering also contribute. It is interesting to see that when a is increased to 10 nm, the electron-BP scattering is the largest spin relaxation mechanism only at high magnetic fields. For 0.4 T $< B < 1$ T ($B < 0.4$ T), the direct spin-phonon coupling due to the strain (the first order hyperfine interaction together with the BP) becomes the largest relaxation mechanism respectively. It is also noted that there is no single mechanism which dominates the whole relaxation. Two or three mechanisms are jointly responsible for the spin relaxation. It is indicated that the spin relaxations induced by different mechanisms all increase with B . This can be understood from a perturbation argument: since the spin relaxation between two Zeeman split states for each mechanism is proportional to $n_q(\Delta E)^m$ (ΔE is the Zeeman splitting) with $m = 5$ for electron-BP scattering due to the deformation potential and for the second-order process of the hyperfine interaction together with the electron-BP scattering due to the deformation potential $V_{eI-ph}^{(3)}$; $m = 3$ for electron-BP scattering due to the piezoelectric coupling and for the second-order process of the hyperfine interaction together with the electron-BP scattering due to the piezoelectric coupling $V_{eI-ph}^{(3)}$; and $m = 5$ for the direct spin-phonon coupling due to the strain. The spin relaxation induced by the g -factor fluctuation is proportional to $n_q(\Delta E)^5 B^2$. For most of the cases studied, ΔE is smaller than $k_B T$, hence $n_q \sim \Delta E^{-1}$, and $n_q(\Delta E)^m \sim (\Delta E)^{m-1}$. $m > 1$ hold for all mechanism, therefore the spin relaxation increases with increasing B .

3. Diameter Dependence

We now turn to the investigation of the diameter dependence of the spin relaxation for a small ($a = 5$ nm) and a large ($a = 10$ nm) well widths in Fig. 3a and b respectively for a fixed magnetic field $B = 0.5$ T. It is interesting to see that the relative importance of the spin relaxation mechanism is quite different for small and big well widths. For small well width the electron-BP interaction dominates the spin relaxation when d_0 is large enough. When d_0 is small, the first-order process of the hyperfine interaction together with the electron-BP scattering ($V_{eI-ph}^{(1)}$) becomes dominant. However, for large well width, the electron-BP scattering is unimportant for diameters smaller than 25 nm. For the $a = 10$ nm case, the first-order process of the hyperfine interaction together with the electron-BP scattering ($V_{eI-ph}^{(1)}$) and the direct spin-phonon coupling due to the strain determine the spin relaxation when $d_0 < 20$ nm.

It is seen from the figure that except for the first-order process of the hyperfine interaction together with the electron-BP scattering, the spin relaxation increases with the QD diameter d_0 . This is because for larger QDs,

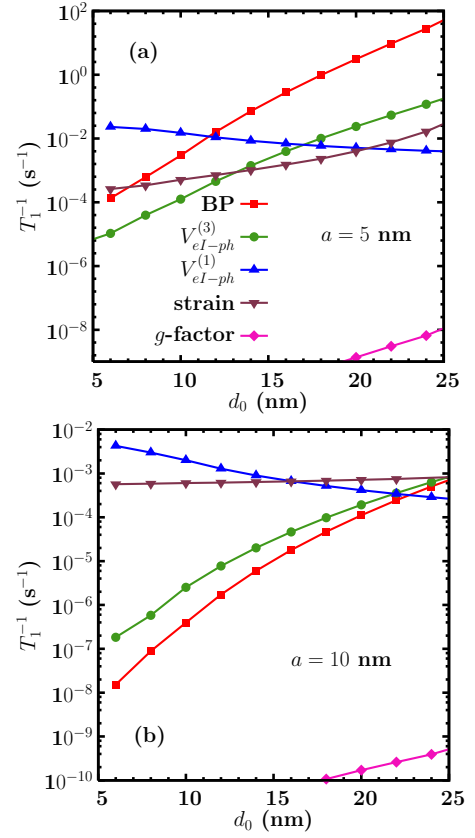


FIG. 3: (Color online) T_1^{-1} induced by different mechanisms *vs.* the effective diameter d_0 at $B = 0.5$ T and (a) $a = 5$ nm and (b) 10 nm. $T = 4$ K. Curves with \blacksquare — T_1^{-1} induced by the electron-BP scattering; Curves with \bullet — T_1^{-1} induced by the second-order process of the hyperfine interaction together with the BP ($V_{eI-ph}^{(3)}$); Curves with \blacktriangle — T_1^{-1} induced by the first-order process of the hyperfine interaction together with the BP ($V_{eI-ph}^{(1)}$); Curves with \blacktriangledown — T_1^{-1} induced by the direct spin-phonon coupling due to the strain; Curves with \blacklozenge — T_1^{-1} induced by the g -tensor fluctuation.

more energy levels are engaged in the spin-flip scattering. Consequently the total spin relaxation increases. However, the spin relaxation from $V_{eI-ph}^{(1)}$ decreases with the diameter. This is because $V_{eI-ph}^{(1)}$ contains the term $\nabla_{\mathbf{r}}$ [Eq. (19)] which decreases with the increase of d_0 .

B. Spin Dephasing Time T_2

In this subsection, we investigate the spin dephasing time for different well widths, magnetic fields and QD diameters. As in the previous subsection, the contributions of the different mechanisms to the spin dephasing are compared.

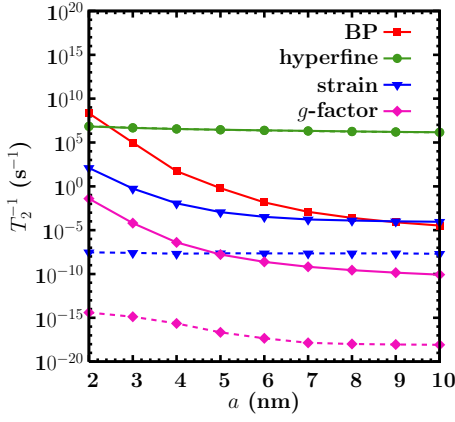


FIG. 4: (Color online) T_2^{-1} induced by different mechanisms with (solid curves) and without (dashed curves) the SOC *vs.* the well width at $B = 0.5$ T and $d_0 = 20$ nm. $T = 4$ K. Curve with ■ — T_2^{-1} induced by the electron-BP interaction; Curves with ● — T_2^{-1} induced by the hyperfine interaction; Curves with ▲ — T_2^{-1} induced by the direct spin-phonon coupling due to the strain; Curves with ◆ — T_2^{-1} induced by g -tensor fluctuation.

1. Well Width Dependence

In Fig. 4 the well width dependence of the spin dephasing induced by different mechanisms is investigated. In the calculations $B = 0.5$ T and $d_0 = 20$ nm. It can be seen that the spin dephasing decreases with the well width and the hyperfine interaction is dominant except for very small well widths (around 2 nm in the figure) where the electron-BP interaction has larger contribution. These features can be understood as following: As $H_{so} \propto a^{-2}$, the SOC decreases quickly with a , which leads to the sharp decrease of spin dephasing induced by the electron-BP scattering. For the hyperfine interaction, the scattering coefficient $A_j = A|\Psi(\mathbf{r}_j)|^2$ changes with the nucleus position \mathbf{r}_j and the decay of $|\langle S_+ \rangle_t|$ is mainly determined by $\nabla_{\mathbf{r}}|\Psi(\mathbf{r})|^2$, which decreases with the increase of a . Consequently, the spin dephasing induced by the hyperfine interaction decreases with a . However, the spin dephasing induced by the electron-BP scattering decreases much faster than that induced by the hyperfine interaction. As a result, when the well width is wide, the hyperfine interaction becomes dominant. It is also noted that the spin dephasing from the direct spin-phonon coupling due to the strain and from the g -tensor fluctuation is negligible. Therefore, in the following figures, we do not consider these two contributions.

Similar to Fig. 1, the SOC is always included in the computation as it has large effect on the eigen-energy and eigen-wavefunction of the electrons. The spin dephasings calculated without the SOC for the hyperfine interaction, the direct spin-phonon coupling due to the strain and the g -factor fluctuation are also shown in Fig. 4 as dashed curves. It can be seen from the figure that for the spin

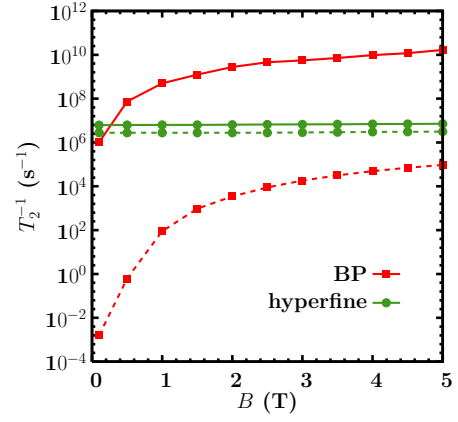


FIG. 5: (Color online) T_2^{-1} induced by the electron-BP scattering and the hyperfine interaction *vs.* the magnetic field B at $d_0 = 20$ nm for $a = 2$ nm (solid curves) and 5 nm (dashed curves). $T = 4$ K. Curves with ■ — T_2^{-1} induced by the electron-BP interaction; Curves with ● — T_2^{-1} induced by the hyperfine interaction.

dephasings induced by the direct spin-phonon coupling due to the strain and by the g -tensor fluctuation, the contributions with the SOC are much larger than those without. This is because when the SOC is included, the fluctuation of the effective field induced by both mechanisms becomes much stronger. However, what should be emphasized is that the spin dephasings induced by the hyperfine interaction with and without the SOC are nearly the same (the solid and the dashed curves nearly coincide). That is because the change of the wavefunction $\Psi(\mathbf{r})$ due to the SOC is very small (less than 1 % in our condition) and therefore $\nabla_{\mathbf{r}}|\Psi(\mathbf{r})|^2$ is almost unchanged when the SOC is neglected.

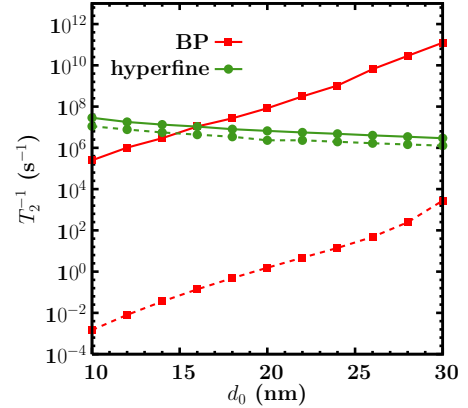


FIG. 6: (Color online) T_2^{-1} induced by the electron-BP scattering and the hyperfine interaction *vs.* the effective diameter d_0 at $B = 0.5$ T for $a = 2$ nm (solid curves) and 5 nm (dashed curves). $T = 4$ K. Curves with ■ — T_2^{-1} induced by the electron-BP interaction; Curves with ● — T_2^{-1} induced by the hyperfine interaction.

2. Magnetic Field Dependence

We then investigate the magnetic field dependence of the spin dephasing induced by the electron-BP scattering and by the hyperfine interaction at two different well widths. In the calculations, $d_0 = 20$ nm. It is interesting to see from Fig. 5 that the relative importance of the electron-BP scattering and the hyperfine interaction is quite different for small and large well widths. For small width (2 nm in the figure), the electron-BP interaction is dominant except at very low magnetic field ($B = 0.1$ T in the figure). However, for large well width, the hyperfine interaction always gives the largest contribution. It is further noticed that the spin dephasing induced by the electron-BP scattering increases with the magnetic field whereas that induced by the hyperfine interaction decreases with the magnetic field. Besides spin relaxation, the spin-flip transition also contribute to spin dephasing. As has been demonstrated in Sec. IIA, the electron-BP scattering induced spin-flip transition rate increases with increasing magnetic field. Therefore the spin dephasing rate increases with increasing magnetic field. In contrast, T_2^{-1} induced by the hyperfine interaction decreases with the magnetic field. This is because when B becomes larger, the fluctuation of the effective magnetic field due to the surrounding nuclei becomes insignificant compared to the much larger applied magnetic field. Therefore, the contribution from the hyperfine interaction to the dephasing is suppressed.

3. Diameter Dependence

In Fig. 6 the spin dephasings induced by the electron-BP scattering and the hyperfine interaction are plotted as function of the diameter d_0 for a small ($a = 2$ nm) and a large ($a = 5$ nm) well widths. In the calculation, $B = 0.5$ T. It is interesting to see from the figure for small well width the hyperfine interaction has the largest

contribution when d_0 is small enough. When d_0 is larger than 16 nm, the electron-BP scattering becomes dominant. However, for large well width, the hyperfine interaction always has the largest contribution. This comes from that the spin dephasing induced by the electron-BP scattering decreases faster with the well width than that induced by the hyperfine interaction as explained before.

It is also noted the spin dephasing induced by the electron-BP scattering increases with d_0 whereas that induced by the hyperfine interaction decreases with it. This is understood that for larger QDs, the energy levels become closer to each other. Therefore the scattering between two orbital energy levels becomes easier. Moreover, for closer energy levels, each Zeeman sublevel mixes stronger with other levels with opposite spin, which also leads to a faster spin relaxation. As a result, the spin dephasing becomes larger. However, with the increase of d_0 the wavefunction of the electron becomes more homogeneous, which means $\nabla_{\mathbf{r}}|\Psi(\mathbf{r})|^2$ becomes smaller. Therefore the fluctuation strength of the effective field due to the second-process of spin-flip interaction between the electron and any two nuclei in different position becomes weaker. This leads to a smaller spin dephasing.

IV. FERMI-GOLDEN-RULE APPROACH VS. EQUATION-OF-MOTION APPROACH

We now compare the spin relaxation from the Fermi Golden rule approach widely used in the literature with the result from the equation-of-motion approach addressed above. We focus only on the spin relaxation due to the electron-BP interaction in this section.

We first show the difference between these two approaches when only two energy levels $|\ell_1\rangle$ and $|\ell_2\rangle$ are considered. The equation of motion of the density matrix elements $\rho_{\ell_1\ell_1}^e$, $\rho_{\ell_1\ell_2}^e$, $\rho_{\ell_2\ell_1}^e$ and $\rho_{\ell_2\ell_2}^e$ can be derived from Eq. (7), resulting in

$$\frac{d}{dt} \begin{bmatrix} \rho_{\ell_1\ell_1}^e \\ \rho_{\ell_1\ell_2}^e \\ \rho_{\ell_2\ell_1}^e \\ \rho_{\ell_2\ell_2}^e \end{bmatrix} = - \begin{bmatrix} D_1 & 0 & 0 & -D_2 \\ 0 & \frac{D_1+D_2}{2} - i(\varepsilon_{\ell_1} - \varepsilon_{\ell_2}) & 0 & 0 \\ 0 & 0 & \frac{D_1+D_2}{2} - i(\varepsilon_{\ell_2} - \varepsilon_{\ell_1}) & 0 \\ -D_1 & 0 & 0 & D_2 \end{bmatrix} \begin{bmatrix} \rho_{\ell_1\ell_1}^e \\ \rho_{\ell_1\ell_2}^e \\ \rho_{\ell_2\ell_1}^e \\ \rho_{\ell_2\ell_2}^e \end{bmatrix} \quad (27)$$

in which

$$\left\{ \begin{matrix} D_1 \\ D_2 \end{matrix} \right\} = \frac{2\pi}{\hbar} \sum_{\mathbf{q}\eta} |M_{\mathbf{q}\eta}|^2 |\langle \ell_1 | e^{i\mathbf{q}\cdot\mathbf{r}} | \ell_2 \rangle|^2 [n_{\mathbf{q}} \delta(\varepsilon_{\ell_1} - \varepsilon_{\ell_2} \pm \hbar\omega_{\mathbf{q}\eta}) + (n_{\mathbf{q}} + 1) \delta(\varepsilon_{\ell_1} - \varepsilon_{\ell_2} \mp \hbar\omega_{\mathbf{q}\eta})] . \quad (28)$$

From Eq. (27), one has

$$\frac{d}{dt} (\rho_{\ell_1\ell_1} - \rho_{\ell_2\ell_2}) = -(D_1 + D_2)(\rho_{\ell_1\ell_1} - \rho_{\ell_1\ell_2}) + (D_2 - D_1)N_0 , \quad (29)$$

where $N_0 = \rho_{\ell_1\ell_1} + \rho_{\ell_2\ell_2}$ is a constant. As $S_z(t) = \text{Tr}(S_z \rho^e(t)) = \sum_{i,j=\{\ell_1,\ell_2\}} \langle j|S_z|i\rangle \rho_{i,j}^e$, when the portion of the minority spin polarization of the two states can be neglected, $S_z(t) \approx \hbar(\rho_{\ell_1\ell_1} - \rho_{\ell_2\ell_2})/2$. Therefore,

$$1/T_1^{EM} \approx D_1 + D_2. \quad (30)$$

On the other hand, the spin relaxation from $|\ell_2\rangle$ to $|\ell_1\rangle$ obtained from the Fermi Golden rule^{17,54,55,56} reads

$$1/T_1^{FGR} = \frac{2\pi}{\hbar} \sum_{\mathbf{q}\eta} |M_{\mathbf{q}\eta}|^2 |\langle \ell_1 | e^{i\mathbf{q}\cdot\mathbf{r}} | \ell_2 \rangle|^2 [n_{\mathbf{q}} \delta(\varepsilon_{\ell_1} - \varepsilon_{\ell_2} - \hbar\omega_{\mathbf{q}\eta}) + (n_{\mathbf{q}} + 1) \delta(\varepsilon_{\ell_1} - \varepsilon_{\ell_2} + \hbar\omega_{\mathbf{q}\eta})]. \quad (31)$$

By investigating the ratio

$$R = T_1^{FGR}/T_1^{EM}, \quad (32)$$

one is able to study the difference between the two approaches. If $\varepsilon_{\ell_2} > \varepsilon_{\ell_1}$, one has $R = (2n_{\mathbf{q}} + 1)/(n_{\mathbf{q}} + 1)$. However, if $\varepsilon_{\ell_2} < \varepsilon_{\ell_1}$, $R = (2n_{\mathbf{q}} + 1)/n_{\mathbf{q}}$. Here $n_{\mathbf{q}} \equiv \{\exp[\varepsilon_{\ell_2} - \varepsilon_{\ell_1}]/(k_B T)] - 1\}^{-1}$.

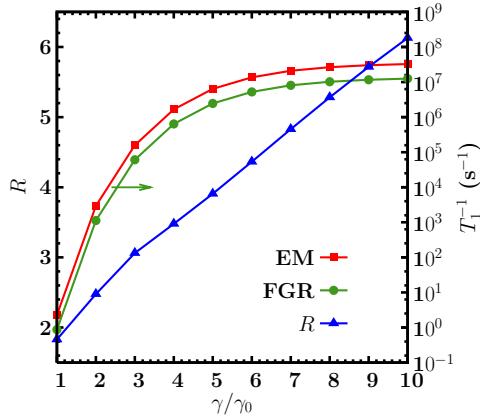


FIG. 7: (Color online) The ratio R and the spin relaxation *vs.* the SOC strength γ at $B = 0.5$ T, $a = 5$ nm and $d_0 = 20$ nm. $T = 4$ K. Curve with \blacktriangledown — the ratio R ; Curve with \blacksquare — T_1^{-1} obtained from the equation-of-motion (EM) approach; Curve with \bullet — T_1^{-1} obtained from the Fermi Golden rule (FGR) approach. Note the scale of the spin relaxation is on the right hand side of the frame.

We first consider the spin relaxation between the lowest three energy levels $|\ell\rangle$ ($\ell = 1, 2, 3$) to show how R varies with the SOC parameter γ . From the perturbation method, the three spin mixed states can be written as^{17,41}

$$|1\rangle = |00+\rangle|1_z\rangle - \mathcal{B}_1|0-1-\rangle|1_z\rangle, \quad (33)$$

$$|2\rangle = |00-\rangle|1_z\rangle - \mathcal{A}_1|01+\rangle|1_z\rangle, \quad (34)$$

$$|3\rangle = |01+\rangle|1_z\rangle + \mathcal{A}_1|00-\rangle|1_z\rangle, \quad (35)$$

with $\mathcal{A}_\lambda = i\alpha\gamma\langle P_z^2 \rangle_\lambda (1 - eB/(2\hbar\alpha^2))/(E_{0-1-, \lambda} - E_{00+, \lambda})$ and $\mathcal{B}_\lambda = i\alpha\gamma\langle P_z^2 \rangle_\lambda (1 + eB/(2\hbar\alpha^2))/(E_{0-1+, \lambda} - E_{00-, \lambda})$. $|nl\sigma\rangle|\lambda\rangle$ and $E_{nl\sigma, \lambda}$ represent the eigen state and eigen energy of $\frac{\mathbf{p}^2}{2m^*} + V_c(\mathbf{r}) + H_z$, respectively, $\langle P_z^2 \rangle_\lambda$ is the average value of P_z^2 in the λ -th subband along the z direction.

In the above equations, $\omega_B = eB/(2m^*)$, $\Omega = \sqrt{\omega_0^2 + \omega_B^2}$ and $\alpha = \sqrt{m^*\Omega/\hbar}$. If we consider the spin relaxation from a spin-down state to a spin-up state, the spin relaxation can only happen from $|2\rangle$ to $|1\rangle$ and $|2\rangle$ to $|3\rangle$ when only the lowest three levels are considered. As $\varepsilon_2 > \varepsilon_1$, $R_{21} = (2n_{\mathbf{q}} + 1)/(n_{\mathbf{q}} + 1)$ between $|1\rangle$ and $|2\rangle$ with $n_{\mathbf{q}} = \{\exp[\Delta E_{12}/(k_B T)] - 1\}^{-1}$. When spin relaxation from $|2\rangle$ to $|3\rangle$ is considered, $R_{23} = (2n_{\mathbf{q}} + 1)/n_{\mathbf{q}}$ as $\varepsilon_2 < \varepsilon_3$, where $n_{\mathbf{q}} = \{\exp[\Delta E_{23}/(k_B T)] - 1\}^{-1}$. For finite T , the spin relaxation time from both approaches can be quite different. From the perturbation, we obtain^{17,41}

$$\Delta E_{12} = 2E_B + \alpha^2 \gamma^2 \langle P_z^2 \rangle_1^2 \left[\frac{(1 + eB/(2\hbar\alpha^2))^2}{\hbar\Omega - (\hbar\omega_B - 2E_B)} - \frac{(1 - eB/(2\hbar\alpha^2))^2}{\hbar\Omega + (\hbar\omega_B - 2E_B)} \right], \quad (36)$$

$$\Delta E_{23} = \hbar\Omega - \hbar\omega_B + 2E_B + \alpha^2 \gamma^2 \langle P_z^2 \rangle_1^2 \frac{1 + eB/(2\hbar\alpha^2)}{\hbar\Omega - \hbar\omega_B + 2E_B}, \quad (37)$$

where $E_B = \frac{1}{2}g\mu_B B$ is the Zeeman splitting energy. It is seen from the above equations that both ΔE_{12} and ΔE_{23} increase with the SOC parameter γ . Therefore, as $n_{\mathbf{q}}$ may change from $+\infty$ to 0 if ΔE_{12} varies from 0 to $+\infty$, the ratio R_{21} varies from 2 to 1. However, R_{23} varies from 2 to $+\infty$ if $n_{\mathbf{q}}$ changes from $+\infty$ to 0 with ΔE_{23} . Specifically, when $\gamma = \gamma_0$, the energy difference ΔE_{12} between the lowest two energy levels is about 2.5×10^{-5} eV, which is smaller than $k_B T$ (when $T = 4$ K). Therefore $R_{21} \sim 1.95$. However, when γ is increased to $10\gamma_0$, $\Delta E_{12} \sim 9 \times 10^{-4}$ eV, which is larger than $k_B T$ and consequently $R_{21} \sim 1.3$. Therefore, R_{21} decreases with γ . Nevertheless, for spin relaxation between $|2\rangle$ and $|3\rangle$, when $\gamma = \gamma_0$, $\Delta E_{23} \sim 1 \times 10^{-4}$ eV which is larger than $k_B T$, $R_{23} \sim 2.28$. For $\gamma = 10\gamma_0$, $\Delta E_{23} \sim 1.5 \times 10^{-3}$ eV and $R_{23} \sim 19$. Moreover, it should be stressed that when the SOC is large, the portion of the minority spin can not be neglected. Consequently, Eq. (30) is no longer valid. For example, if we take $|\ell_1\rangle = |2\rangle$ and $|\ell_2\rangle = |3\rangle$, then $S_z = -(1 - \mathcal{A}_1^2)(\rho_{11}(t) - \rho_{22}(t)) - 2\mathcal{A}_1(\rho_{12}(t) + \rho_{21}(t))$, where the effect of ρ_{12} and ρ_{21} to S_z can not be neglected. Hence the spin relaxation time from the equation-of-motion approach becomes more complicated. In general the off-diagonal parts ρ_{12} and ρ_{21} relax faster than the diagonal one in the condition we considered, therefore including this effect the spin relaxation becomes

faster.

It is interesting to see that when the temperature is near zero, where only the lowest two Zeeman sub-levels are relevant, $\langle 1|S_z|2 \rangle$ is exactly zero according to Eq (35). This is because the SOC, regardless of the Rashba or Dresselhaus coupling, only mixes states with *both* different spin *and* different orbital states. Therefore $\langle 1|S_z|2 \rangle$ is exactly zero as a consequence of the orthogonality of the orbital part of the wavefunction. Therefore $1/T_1^{EM} = D_1 + D_2$ is valid exactly and $T_1^{EM} = T_1^{FGR}$ as $R = (2n_q + 1)/(q+1) = 1$ when $T = 0$.

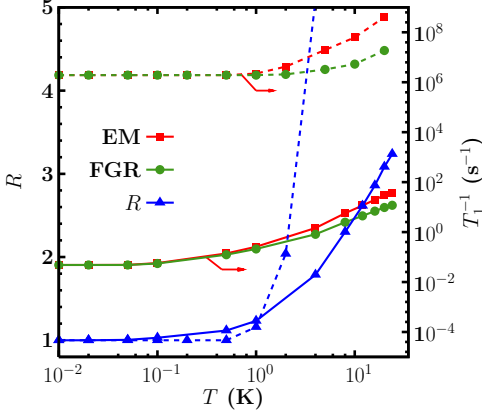


FIG. 8: (Color online) The ratio R and spin relaxation for $\gamma = \gamma_0$ (solid curves) and $10\gamma_0$ (dashed curves) vs. the temperature T at $B = 0.5$ T, $a = 5$ nm and $d_0 = 20$ nm. Curves with \blacktriangledown — the ratio R ; Curves with \blacksquare — T_1^{-1} obtained by the equation-of-motion (EM) approach; Curves with \bullet — T_1^{-1} obtained by the Fermi Golden rule (FGR) approach. Note the scale of the spin relaxation is on the right hand side of the frame.

We further turn to the situation where all the energy levels are included. In Fig. 7, the ratio R from Eq. (32) and the inverse of the spin relaxation times from the different approaches are plotted against the SOC strength γ . $T = 4$ K in the calculation. It can be seen that when $\gamma = \gamma_0$, $R \sim 1.6$. However, R increases with γ quickly and when $\gamma = 10\gamma_0$, the spin relaxation obtained from our equation-of-motion approach is about 6.2 times that obtained from the Fermi-golden-rule approach. This is because when sufficient energy levels are considered, the spin relaxations from the spin-up (spin-down) states to the spin-down (spin-up) states include not only the contribution from the higher energy levels to the lower energy ones, but also the contribution from the opposite direction. As analyzed before, if the energy of the initial state is below the one of the final state, $R = (2n_q + 1)/n_q$, which increases quickly with γ .

The underlying physics can be understood as follows: When the SOC is small, for each spin mixed state one can figure out the majority spin polarization. Taking the case with $\gamma = \gamma_0$ as an example, the proportion of the minority spin polarization is no more than 1 % for the

lowest few levels. However, for large SOC, distinguishing the majority spin polarization becomes impossible for the spin mixed states. For example, when $\gamma = 10\gamma_0$, the proportions of the majority and the minority spin polarizations are about 53 % and 47 % respectively for the lowest state. Therefore, in this case, the Fermi golden rule is inapplicable for calculating the spin relaxation time.

We further compare the spin relaxations obtained from the two methods at different temperatures. In the calculation, two cases, *i.e.*, $\gamma = \gamma_0$ and $\gamma = 10\gamma_0$, are considered. In Fig. 8, the spin relaxations and their ratio R are plotted against temperature T . Sufficient energy levels are included in the calculation. It is seen from the figure that for $\gamma = \gamma_0$, when the temperature is smaller than 0.07 K, $R \approx 1$. This means that the spin relaxations obtained from the two approaches are identical at very low temperature. However, when T increases, R increases with T and when $T = 24$ K, $R \sim 3.2$. This is because at very low temperature, the electron only distributes in the lowest two energy levels. Therefore, according to our previous discussion, $T_1^{-1} = D_1 + D_2$ and $R = R_{21} \sim 1$ when $T \sim 0$ regardless of the value of γ . When the temperature increases, the electron distributes in many higher energy levels, where the SOC strengths are stronger. Consequently, R is larger in this case. The underlying physics is that, the spin relaxation calculated via the Fermi-golden-rule approach tackles only the relaxation between two spin mixed states, instead of that between the spin-up and spin-down states. Hence, the spin relaxation obtained from the Fermi-golden-rule approach is smaller than that obtained from the equation-of-motion approach at high temperature. It is further noticed in the figure that for larger SOC parameter ($10\gamma_0$ in our case), the ratio $R \sim 22$ when $T = 20$ K. This is because for high temperature, electron distributes into higher energy levels, where the SOC is strong. Hence the effect of off-diagonal terms of ρ to S_z can not be neglected. It is also noticed that the temperature at which R decreases to 1 is larger than that for $\gamma = \gamma_0$. This is because when γ increases, the energy difference ΔE_{12} between the lowest two energy levels becomes larger. Therefore, relative larger T can ensure $n_q \sim 0$.

In brief, the Fermi-golden-rule approach is only valid when the temperature is around zero. For stronger SOC strength, the temperature at which the Fermi-golden-rule approach is valid becomes higher. At high temperature, one should use the equation-of-motion approach to calculate the spin relaxation time.

V. TEMPERATURE DEPENDENCE OF T_1/T_2

In this section, we compare the relative magnitudes of the spin relaxation time and the spin dephasing time. We consider a QD with $d_0 = 30$ nm, where the largest contribution to both spin relaxation and spin dephasing comes from the electron-BP scattering (see Fig. 3a and Fig. 6). In Fig. 9, it is interesting to find that when the

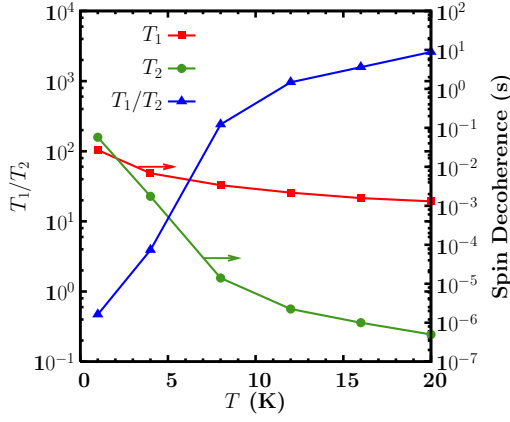


FIG. 9: (Color online) Spin relaxation time T_1 , spin dephasing time T_2 and T_1/T_2 against temperature T . $\gamma = \gamma_0$, $B = 0.5$ T, $a = 5$ nm and $d_0 = 30$ nm. Note the scale of T_1 and T_2 is at the right hand side of the frame.

temperature is low ($T = 1$ K in the figure), $T_2 = 2T_1$, which is in agreement with the main conclusion in Ref. 19. However, when T is increased, T_1/T_2 increases very quickly with it and when T is 20 K, $T_1/T_2 \sim 2 \times 10^3$. This is understood from the fact that when T is low (1 K in our case), the electron mostly distributes in the lowest two Zeeman sublevels. As the SOC strength is small ($\gamma = \gamma_0$), then from Eq. (27), one has

$$\frac{d}{dt}S_x(t) \approx -\frac{D_1 + D_2}{2}S_x + (\varepsilon_2 - \varepsilon_1)S_y, \quad (38)$$

concerning only the lowest two Zeeman sublevels. Consequently, according to Eq. (30), $T_2^{-1} = (D_1 + D_2)/2 = T_1^{-1}/2$.¹⁹ When the temperature becomes higher, more energy levels are involved, and the spin dephasing between two energy levels whose majority spin polarizations are the same are included.²⁴ However, the spin relaxation is only related to the spin-flip processes. Therefore, the spin dephasing has more scattering channels than the spin relaxation. Furthermore, the spin scattering rate between two energy levels with identical majority spin polarizations is much larger than the one between two energy levels with opposite majority spin polarizations. Therefore, the spin dephasing is much larger than the spin relaxation at high temperature.

VI. CONCLUSION

In conclusion, we have investigated the longitudinal and transversal spin decoherence time T_1 and T_2 , called spin relaxation time and spin dephasing time, in different conditions in GaAs QDs from an equation-of-motion approach. Various mechanisms, including the electron-BP scattering, the hyperfine interaction, the direct spin-phonon coupling due to the strain and the g -factor fluctuation are considered and their relative importance is com-

pared. There is no controversy about that when the spin decoherence induced by electron-BP interaction is considered, SOC must be taken into account. However, when the spin relaxation induced by the hyperfine interaction and the direct spin-phonon coupling due to the strain are considered, SOC is neglected in the literature.^{22,23,35} We have shown that, as SOC has large effect on the eigen-energy and the eigen-wavefunction, the spin relaxation induced by each mechanism with SOC is larger than the one without the SOC, especially the second-process of hyperfine interaction combined with the electron-BP interaction. We demonstrated that as the contributions of the hyperfine interaction combined with the electron-BP interaction, the direct spin-phonon coupling due to strain and the g -factor fluctuation become more pronounced when SOC is included, in some conditions these mechanisms may even be dominant over the spin decoherence process. Therefore, the relative contributions from these mechanisms and the electron-BP interaction change a lot when SOC is included. We also show that SOC also has an important contribution to the spin dephasing induced by the direct spin-phonon coupling due to the strain and the g -factor fluctuation. However, it has little effect on the spin dephasing induced by the hyperfine interaction as the wavefunction almost keeps unchanged with or without SOC.

There is no single mechanism which dominates the spin relaxation and dephasing in all regimes. The relative importance of each mechanism varies with the well width, magnetic field and QD diameter. In particular, the electron-BP scattering has the largest contribution when the well width is small enough and the magnetic field and the QD diameter are large enough. However, in other conditions the first-order and second-order processes of the hyperfine interaction combined with electron-BP scattering, the direct spin-phonon coupling due to the strain also contribute. It is noted that the g -factor fluctuation always has very little contribution to the spin relaxation and can be neglected. For spin dephasing, two mechanisms, *i.e.*, the electron-BP scattering and the hyperfine interaction, give the main contribution. Especially, the electron-BP scattering is dominant when the well width is small and the magnetic field and the QD diameter are large.

We have also discussed the difference between the approaches of equation of motion and Fermi golden rule. We analyzed the difference between the spin relaxations due to the electron-BP scattering together with SOC obtained from the two approaches for different SOC parameters and temperatures. Generally, the two approaches yield the same results when SOC is small and the temperature is low. However, when temperature is away from zero, as the eigen-states are not the pure spin states, the results from the Fermi-golden-rule approach depart from the ones from the equation-of-motion approach. The deviation is larger when SOC is stronger and/or the temperature is higher. Therefore the equation-of-motion approach should be applied to calculate the spin relaxation

and spin dephasing at finite temperatures.

We have also shown the temperature dependence of the ratio T_1/T_2 . At low temperatures, as the electron only distributes on the lowest two Zeeman split levels, $T_2 = 2T_1$. However, for high temperatures, the electron occupies higher energy levels and more energy levels are involved. The spin dephasing is greatly enhanced as two energy levels with identical majority spin polarizations contribute to the spin dephasing. Moreover, this contribution is much larger than the one between two energy levels whose majority polarizations are opposite. However, the spin relaxation is only related to the spin-flip process. Therefore, the spin dephasing has more scattering channels than the spin relaxation. Consequently

$$T_1 \gg T_2.$$

Acknowledgments

This work was supported by the Natural Science Foundation of China under Grant No. 10574120, the National Basic Research Program of China under Grant No. 2006CB922005, the Innovation Project of Chinese Academy of Sciences and SRFDP. The authors would like to thank Dan Csontos for his critical reading of this manuscript. Y.Y.W. would like to thank J. L. Cheng for valuable discussions.

* Author to whom correspondence should be addressed;
Electronic address: mwwwu@ustc.edu.cn

† Mailing Address

- ¹ *Semiconductor Spintronics and Quantum Computation*, edited by D. D. Awschalom, D. Loss, and N. Samarth (Springer-Verlag, Berlin, 2002); I. Zutic, J. Fabian, and S. Das Sarma, Rev. Mod. Phys. **76**, 323 (2004).
- ² H.-A. Engel, L. P. Kouwenhoven, D. Loss, and C. M. Marcus, Quantum Information Processing **3**, 115 (2004); D. Heiss, M. Kroutvar, J. J. Finley, and G. Abstreiter, Solid State Commun. **135**, 591 (2005); and references therein.
- ³ D. Loss and D. P. DiVincenzo, Phys. Rev. A **57**, 120 (1998).
- ⁴ R. Hanson, L. P. Kouwenhoven, J. R. Petta, S. Tarucha, and L. M. K. Vandersypen, cond-mat/0610433.
- ⁵ J. M. Taylor, H.-A. Engel, W. Dür, A. Yacoby, C. M. Marcus, P. Zoller, and M. D. Lukin, Nature Physics **1**, 177 (2005).
- ⁶ D. Paget, G. Lample, B. Sapoval, and V. I. Safarov, Phys. Rev. B **15**, 5780 (1977).
- ⁷ G. E. Pikus and A. N. Titkov, *Optical Orientation* (Berlin, Springer, 1984).
- ⁸ G. Dresselhaus, Phys. Rev. **100**, 580 (1955).
- ⁹ Y. Bychkov and E. I. Rashba, J. Phys. C **17**, 6039 (1984).
- ¹⁰ Laura M. Both, Phys. Rev. **118**, 1534 (1960).
- ¹¹ F. Meier and B. P. Zakharchenya, *Optical Orientation* (North-Holland, Amsterdam, 1984).
- ¹² A. V. Khaetskii and Y. V. Nazarov, Physica E **6**, 470 (2000).
- ¹³ A. V. Khaetskii and Y. V. Nazarov, Phys. Rev. B **61**, 12639 (2000).
- ¹⁴ A. V. Khaetskii and Y. V. Nazarov, Phys. Rev. B **64**, 125316 (2001).
- ¹⁵ L. M. Woods, T. L. Reinecke, and Y. Lyanda-Geller, Phys. Rev. B **66**, 161318 (2002).
- ¹⁶ R. de Sousa and S. Das Sarma, Phys. Rev. B **68**, 155330 (2003).
- ¹⁷ J. L. Cheng, M. W. Wu, and C. Lü, Phys. Rev. B **69**, 115318 (2004).
- ¹⁸ D. V. Bulaev and D. Loss, Phys. Rev. B **71**, 205324 (2005).
- ¹⁹ V. N. Golovach, Alexander Khaetskii, and Daniel Loss, Phys. Rev. Lett. **93**, 016601 (2004).
- ²⁰ C. F. Destefani and S. E. Ulloa, Phys. Rev. B **72**, 115326 (2005).

- ²¹ P. San-Jose, G. Zarand, A. Shnirman, and G. Schön, Phys. Rev. Lett. **97**, 076803 (2006).
- ²² S. I. Erlingsson, and Yuli V. Nazarov, Phys. Rev. B **66**, 155327 (2002).
- ²³ V. A. Abalmassov and F. Marquardt, Phys. Rev. B **70**, 075313 (2004).
- ²⁴ Y. G. Semenov and K. W. Kim, Phys. Rev. Lett. **92**, 026601 (2004).
- ²⁵ A. V. Khaetskii, D. Loss, and L. Glazman, Phys. Rev. Lett. **88**, 186802 (2002).
- ²⁶ A. Khaetskii, D. Loss, and L. Glazman, Phys. Rev. B **67**, 195329 (2003).
- ²⁷ J. Schliemann, A. Khaetskii, and D. Loss, J. Phys.: Condens. Matter **15**, R1809 (2003) and references there in.
- ²⁸ W. A. Coish and Daniel Loss, Phys. Rev. B **70**, 195340 (2004).
- ²⁹ Ö Cakir and T Takagahara, cond-mat/0609217.
- ³⁰ C. Deng and X. Hu, cond-mat/0608544.
- ³¹ S. I. Erlingsson and Yuli V. Nazarov, Phys. Rev. B **70**, 205327 (2004).
- ³² N. Shenvi, R. de Sousa, and K. B. Whaley, Phys. Rev. B **71**, 224411 (2005).
- ³³ R. de Sousa, cond-mat/0610716.
- ³⁴ Y. V. Pershin and V. Privman, Nano Lett. **3**, 695 (2003).
- ³⁵ Y. G. Semenov and K. W. Kim, Phys. Rev. B **70**, 085305 (2004).
- ³⁶ W. M. Witzel and S. Das Sarma, Phys. Rev. Lett. **98**, 077601 (2007).
- ³⁷ R. de Sousa, N. Shenvi, and K. B. Whaley, Phys. Rev. B **72**, 045330 (2005).
- ³⁸ J. H. Jiang and M. W. Wu, Phys. Rev. B **75**, 035307 (2007).
- ³⁹ L. M. Roth, Phys. Rev. **118**, 1534 (1960).
- ⁴⁰ B. A. Glavin and K. W. Kim, Phys. Rev. B **68**, 045308 (2003).
- ⁴¹ Y. Y. Wang and M. W. Wu, Phys. Rev. B **74**, 165312 (2006).
- ⁴² V. I. Fal'ko, B. L. Altshuler, and O. Tsyplatyev, Phys. Rev. Lett. **95**, 076603 (2005).
- ⁴³ P. Stano and J. Fabian, Phys. Rev. Lett. **96**, 186602 (2006).
- ⁴⁴ P. Stano and J. Fabian, Phys. Rev. B **74**, 045320 (2006).
- ⁴⁵ H. Westfahl, Jr., A. O. Caldeira, G. Medeiros-Ribeiro, and M. Cerro, Phys. Rev. B **70**, 195320 (2004).
- ⁴⁶ D. V. Bulaev and D. Loss, Phys. Rev. Lett. **95**, 076805

- (2005).
- ⁴⁷ W. H. Lau and M. E. Flatté, Phys. Rev. B **72**, 161311(R) (2005).
- ⁴⁸ T. Fujisawa, D. G. Austing, Y. Tokura, Y. Hirayama, and S. Tarucha, Nature **419**, 278 (2002).
- ⁴⁹ see, *e.g.*, P. N. Argyres and P. L. Kelley, Phys. Rev. **134**, A98 (1964).
- ⁵⁰ M. I. D'yakonov and V. I. Perel', Zh. Eksp. Teor. Fiz. **60**, 1954 (1971) [Sov. Phys. JETP **33**, 1053 (1971)].
- ⁵¹ A. Abragam, *The Principles of Nuclear Magnetism* (Oxford University Press, Oxford, 1961), Chaps. VI and IX.
- ⁵² *Numerical Data and Functional Relationships in Science and Technology*, edited by O. Madelung, M. Schultz, and H. Weiss, Landolt-Börnstein, New Series, Group III, Vol. 17, Pt. a (Springer-Verlag, Berlin, 1982).
- ⁵³ W. Knap, C. Skierbiszewski, A. Zduniak, E. Litwin-Staszewska, D. Bertho, F. Kobbi, J. L. Robert, G. E. Pikus, F. G. Pikus, S. V. Iordanskii, V. Mosser, K. Zekentes, and Yu. B. Lyanda-Geller, Phys. Rev. B **53**, 3912 (1996).
- ⁵⁴ M. Florescu, S. Dickman, M. Ciorga, A. Sachrajda, and P. Hawrylak, Physica E **22**, 414 (2004).
- ⁵⁵ A. M. Alcalde, Q. Fanyao, and G. E. Marques, Physica E **20**, 228 (2004).
- ⁵⁶ C. L. Romano, P. I. Tamborenea, and S. E. Ulloa, Phys. Rev. B **74**, 155433 (2006).